

Original article

Insights from Boltzmann transformation in solving 1D counter-current spontaneous imbibition at early and late time

Pål Østebø Andersen *

Department of Energy Resources, University of Stavanger, 4021 Stavanger, Norway

Keywords:

Counter-current spontaneous imbibition
boltzmann transform
early and late time solutions
square root of time recovery
interpreting spontaneous imbibition data

Cited as:

Andersen, P. Ø. Insights from Boltzmann transformation in solving 1D counter-current spontaneous imbibition at early and late time. *Advances in Geo-Energy Research*, 2023, 7(3): 164-175.
<https://doi.org/10.46690/ager.2023.03.03>

Abstract:

Counter-current 1D spontaneous imbibition in scaled form is investigated using Boltzmann transform before and after water meets the closed boundary (early and late time). At early time the system is self-similar and only depends on position divided by square root of time. At late time it also depends on the interaction with the no-flow boundary and hence a second variable, which is set as the square root of time. Diffusion coefficients shifted to high saturations result in early time spatial saturation profiles with shorter front distance, higher average saturation within the imbibition profile and larger imbibed amount. Strongly water-wet systems have zero oil mobility at the inlet, while mixed-wet systems have finite non-zero mobility. The imbibition rate is proportional to inlet diffusion coefficient, inlet saturation gradient (regarding position divided by square root of time) and inverse square root of time. Accordingly, the saturation gradient is infinite and finite for strongly water-wet and mixed-wet systems. At early time, the profile does not change, thus recovery is proportional to square root of time. When the front meets the no-flow boundary (critical time), the saturation profile deviates from the early time profile first at the no-flow boundary, then towards the inlet. When the inlet gradient changes, imbibition rate declines faster than inverse square root of time. The interaction at the inlet and not the closed boundary, thus determines when recovery stops being proportional to square root of time and explains why such proportionality after critical time is reported. The findings were confirmed by matching experimental data.

1. Introduction

Spontaneous imbibition (SI) refers to capillary force driven displacement of non-wetting fluid by wetting fluid (Morrow and Mason, 2001). This process is highly relevant for recovery of hydrocarbons during water injection, reservoir drive displacement of CO₂ and hydrogen plumes during subsurface storage in porous media and water loss during hydraulic fracturing (Bennion and Bachu, 2010; Makhanov et al., 2014; Zhou et al., 2022). In fractured reservoirs where the permeability contrast is high, SI is especially important (Mattax and Kyte, 1962). In low capillarity reservoirs, mobility control of dominant fractures with foam or other chemicals can be performed to obtain better sweep and storage efficiency (Sæle et al., 2022). SI also permits water to invade zones of high non-wetting phase saturation and create transition zones thus

expanding the extent of injected plumes.

SI can occur counter-currently or co-currently (Bourbiaux and Kalaydjian, 1990; Meng et al., 2019) depending on whether the system is exposed to only wetting phase (called water), or both wetting and non-wetting phase (called oil), respectively. This work considers counter-current SI (COUSI) which is modeled using a capillary diffusion equation with saturation dependent diffusion coefficient. The 1D problem is in focus as SI in other geometries often is approximated to 1D by a characteristic system length (Ma et al., 1997). Andersen (2022) showed that all 1D COUSI problems can be modeled in the same scaled form, and that scaled recovery can be well described using a two-parameter correlation for all relevant shapes of the diffusion coefficient.

It is noteworthy that diffusion and its equation in general form has many applications including heat transfer (Carslaw

and Jaeger, 1947), molecular and chemical transport (Crank and Henry, 1949; Crank, 1979; Cussler, 2009) and oil/gas production (Morrow and Mason, 2001). The results are thus transferable. Boltzmann (1894) showed that the diffusion equation with variable diffusion coefficient can be formulated as an ordinary diffusion equation by expressing it as a function of $x/t^{0.5}$, a combination of the spatial and temporal variables x and t . For a constant coefficient and semi-infinite media, the error function solution was derived. He proposed a solution for estimating the variable dependent diffusion coefficient based on concentration observations and the self-similar form of the equation. See Stenlund (2011) for a summary of classical methods to estimate diffusion coefficients. Crank and Henry (1949) considered adsorbing diffusing species and expressed a solution for concentration implicitly as an integral of the spatial distribution of the diffusion coefficient and constant factor that needed to be determined to obey the initial condition. Larsson (2021) presented various numerical techniques to solve the diffusion equation.

In the SI context McWhorter and Sunada (1990) assumed the self-similar form to hold while expressing the flux as declining with the square root of time. As a result, they obtained general solutions for 1D SI valid for all saturation functions, with the important result that saturation profiles are invariant in shape and that recovery is proportional to the square root of time. Schmid and Geiger (2013) derived a general scaling time based on imbibed volume. Andersen et al. (2020) extended the analytical solution and time scale with viscous coupling effects, which effectively lower fluid mobilities during counter-current flow (Qiao et al., 2018). Andersen (2021) demonstrated that shale gas production with rock- and fluid compressibility, adsorption, gas slippage and permeability reduction could be treated in the same way. Effectively, all these systems thus yield recovery proportional to the square root of time. Deviations from such trends have been used to identify non-standard flow mechanisms (Makhanov et al., 2014; Tantciura et al., 2022). Khan et al. (2018) implemented SI in a commercial simulator and showed that the self-similar early time solution was produced under different conditions. Le Guen and Kovscek (2006) presented experimental saturation profiles they argued did not overlap sufficiently to be self-similar, due to non-equilibrium effects. Cai and Yu (2011) showed that in fractal tortuous media co-current imbibition in capillaries could differ from square root of time trends. Wang and Sheng (2018) showed that systems where SI is combined with advective flow can be self-similar if the advection rate declines with square root of time.

The main limitation of the self-similar solution is that it theoretically is valid only at early time before the traveling front interacts with any closed (or other type) boundaries. During this interaction the system stops acting as infinite and demonstrates a finite production/storage capacity. Recovery against time eventually begins to decline faster than by the square root of time trend. However, many studies have shown that the square root of time trend is a very good approximation until a much higher recovery than at the start of the interaction (Li et al., 2006; March et al., 2016; Andersen, 2021, 2022). Andersen (2022) estimated accurately how high recovery can

be obtained following square root of time, noting that it is only a function of the shape, not magnitude, of the diffusion coefficient of the relevant saturation interval. Coefficients shifted to high water saturations (obtained at high oil-to-water mobility ratio) can result in almost full recovery in this regime.

In this work SI for early- and full-time systems is investigated using the self-similar variable and the resulting advantages and challenges of these formulations are considered. From our review, there seems to be a knowledge gap regarding the self-similar behavior during the transition from early to late time and in full-time solutions. In the full-time system the effects of the closed boundary must be included through a second variable. Some points of interest are: How is the self-similar saturation profile affected by the closed boundary at late times? How is this related to the overall impact on recovery trends? What physical insights and understanding can be gained from presenting the system in this form compared to conventional formulations? First presented in Section 2, is the mathematical system describing 1D COUSI. It is normalized and then early- and full-time formulations based on the self-similar variable are derived. Numerical results are presented based on the different formulations in Section 3 and the paper is concluded in Section 4.

2. Theory

2.1 Mathematical definition

The 1D counter-current spontaneous imbibition problem for oil-water ($i = o, w$) can be formulated as a nonlinear diffusion equation:

$$\phi \partial_t S_w = -\partial_x (K \lambda_o f_w \partial_x P_c), \quad (0 < x < L) \quad (1)$$

where x is position from the inlet, t time since imbibition starts, ϕ is porosity, S_w water saturation, K permeability, $\lambda_i = k_{ri}/\mu_i$ fluid mobility, k_{ri} relative permeability, μ_i viscosity, $f_w = \lambda_w/(\lambda_w + \lambda_o)$ water fractional flow function, P_c capillary pressure, and L system length. The initial condition is a uniform residual water saturation S_{wr} , the open boundary exposed to water at $x = 0$ has a fixed zero capillary pressure and the closed boundary is defined by zero fluid fluxes u_i :

$$S_w(t = 0) = S_{wr}, \quad P_c(x = 0) = 0, \quad u_i|_{x=L} = 0 \quad (2)$$

The main assumptions leading to this description are incompressibility of rock and fluids, homogeneity, immiscible fluids, Darcy's law and negligible gravitational and advective forces compared to capillary forces.

Andersen (2022) showed that all 1D COUSI problems can be scaled to depend on only a dimensionless diffusion coefficient Λ_n with mean 1. A brief derivation is presented, and that system is studied further. Introduce scaled position X , time T , saturations S and S_n and capillary pressure J :

$$X = \frac{x}{L}, \quad T = \frac{t}{\tau}, \quad (3)$$

$$S = \frac{S_w - S_{wr}}{\Delta S_w}, \quad S_n = \frac{S_w - S_{wr}}{S_w^{eq} - S_{wr}}, \quad P_c = \sigma_{ow} J \sqrt{\frac{\phi}{K}}$$

where $\Delta S_w = 1 - S_{or} - S_{wr}$ (S_{or} is residual oil saturation), σ_{ow} is oil-water interfacial tension, τ is a time scale and S_w^{eq} is

the saturation where capillary pressure is zero. The scaled saturation $0 < S < 1$ spans the mobile saturation interval and is used to define saturation functions. However, the scaled saturation $0 < S_n < 1$ defines the saturation interval where imbibition occurs. Define the dimensionless function Λ as:

$$\Lambda = \frac{-k_{rw}k_{ro} \frac{dJ}{dS}}{k_{rw} \sqrt{\frac{\mu_o}{\mu_w}} + k_{ro} \sqrt{\frac{\mu_w}{\mu_o}}} \quad (4)$$

This function is the saturation dependent part of the capillary diffusion coefficient. Divide this function by its mean $\bar{\Lambda}$ over imbibing saturations to define a normalized function Λ_n with mean 1:

$$\Lambda_n(S_n) = \frac{\Lambda(S)}{\bar{\Lambda}}, \quad \bar{\Lambda} = \int_{S_n=0}^1 \Lambda(S) dS_n \quad (5)$$

Λ_n (and Λ) depend on the saturation functions k_{ri} and J and viscosity ratio, but no other parameters. Define the time scale τ by:

$$\tau = \frac{\Delta S_w L^2 \sqrt{\mu_o \mu_w}}{\sigma_{ow} \bar{\Lambda}} \sqrt{\frac{\phi}{K}} \quad (6)$$

Based on the scaling and definitions above the system in Eqs. (1) and (2) can be written as:

$$\partial_T S_n = \partial_X (\Lambda_n(S_n) \partial_X S_n) \quad (7)$$

$$S_n(T=0) = 0, \quad S_n(X=0) = 1, \quad [\Lambda_n(S_n) \partial_X S_n]_{X=1} = 0 \quad (8)$$

where only the diffusion coefficient $\Lambda_n(S_n)$ varies from one problem to another, depending on saturation functions and viscosity ratio, but not other properties (Andersen 2022). Other parameters (permeability, critical saturations, etc) are required only to unscale the solution. Scaled saturation S_n ranges from 0 to 1 during SI. The recovery factor (RF) is the fraction produced oil of oil that can be produced by SI and thus equals mean scaled saturation:

$$\text{RF} = \bar{S}_n \quad (9)$$

In this work, 1D COUSI solutions of the scaled system are investigated by means of self-similar variables at early and late times.

2.1.1 Self-similar early time solution

First, assume the imbibing water saturation profile has not reached the closed boundary (defined as the critical time T_c). This period is referred to as early time ($T < T_c$). The aim is a solution approach that incorporates important features of the system and directly returns important output parameters. To do so, introduce the Boltzmann variable Z which is related to the space and time variables and derivatives through:

$$Z = XT^{-0.5}, \quad \partial_T = -0.5ZT^{-1} \partial_Z, \quad \partial_X = T^{-0.5} \partial_Z \quad (10)$$

and results in the following expression of the differential Eq. (7) and associated conditions Eq. (8) (except for the closed boundary):

$$Z \partial_Z S_n = -2 \partial_Z (\Lambda_n(S_n) \partial_Z S_n) \quad (11)$$

$$S_n(Z = \infty) = 0, \quad S_n(Z = 0) = 1 \quad (12)$$

A key advantage of expressing the system in this way is that at early time the system does not interact with the closed boundary and hence only depends on Z as an ordinary differential equation. The one solution $S_n(Z)$ to this system thus represents all space-time solutions at early time.

McWhorter and Sunada (1990) derived an analytical solution for early time, which was reformulated to the scaled form of Eq. (13) in Andersen (2022) as follows:

$$X(S_n) = 2AF'(S_n)T^{0.5}, \quad T_{cr}^{0.5} = \frac{1}{2AF'(S_n=0)} \quad (13)$$

The first equation states that the position of a saturation is proportional to the square root of time, a constant A and the saturation derivative of a function $F(S_n)$. The second equation defines the critical time at which the fastest saturation reaches the closed boundary at $X = 1$. From this, express the profile in terms of Z and define the profile's largest Z and its relation to the critical time as:

$$\begin{aligned} Z(S_n) &= 2AF'(S_n), \\ Z_{cr} &= \frac{X(S_n=0)}{T^{0.5}} = \frac{1}{T_{cr}^{0.5}} = 2AF'(S_n=0) \end{aligned} \quad (14)$$

The recovery RF_{cr} when meeting the boundary (which also equals the average saturation behind the front position) is (Andersen 2022):

$$\text{RF}_{cr} = 2AT_{cr}^{0.5} = \frac{1}{F'(S_n=0)} \quad (15)$$

The recovery factor during the early time period is given by the area of the imbibed profile, which is the average saturation of the profile, RF_{cr} , times the distance of the profile, Z_{cr} , divided by the distance of the system $1/Y \geq Z_{cr}$.

$$\text{RF}_{early}(Y) = 2AT^{0.5} = \text{RF}_{cr} Z_{cr} Y, \quad (0 < Y \leq \frac{1}{Z_{cr}}) \quad (16)$$

Note that only Y is non-constant above and that an increment in Y gives a proportional increment in RF .

2.1.2 Solution for all times

At late time, defined as after the saturation front has reached the no-flow boundary, the solution is affected by a second variable. Especially consider that $Z(X=1) = 1/T^{0.5}$ reflects the boundary location and how long the process has been ongoing, while the variable $Z = X/T^{0.5}$, obeying $0 < Z < 1/T^{0.5}$ reflects the positions between the inlet and closed boundary at that time. For convenience select the second variable as $Y = 1/Z(X=1) = T^{0.5}$ and use it together with Z , i.e., $S_n = S_n(Z, Y)$. When reformulating Eq. (7) Z is used in the spatial derivatives (as in Eq. (10)) and Y in the temporal derivative:

$$Y = T^{0.5}, \quad \partial_T = 0.5T^{-0.5} \partial_Y \quad (17)$$

The system can then be written as:

$$\partial_Y S_n = \frac{2}{Y} \partial_Z (\Lambda_n(S_n) \partial_Z S_n), \quad \left(0 < Z < \frac{1}{Y}\right) \quad (18)$$

$$\begin{aligned} S_n(Z, Y=0) = 0, \quad S_n(Z=0, Y) = 1 \\ [\Lambda_n(S_n) \partial_Z S_n]_{Z=1/Y} = 0 \end{aligned} \quad (19)$$

This system can be solved from zero time or as a continuation of the solution from the early time system Eqs. (11) and (12).

2.2 Imbibition rate

From Eq. (7), note that the scaled flux q_0 of water imbibing into the system at the open boundary is:

$$q_0 = -\Lambda_n(S_n) \partial_X S_n |_{x=0} = [-\Lambda_n(S_n) \partial_Z S_n |_{Z=0}] T^{-0.5} \quad (20)$$

The last equality follows directly from the definition of Z . During the early time / infinite-acting period the inlet flux is proportional to $T^{-0.5}$ which is consistent with the above expression as the saturation profile against Z is fixed during that period. However, at late time the saturation profile will no longer only depend on Z . The saturation is at all times fixed at $Z=0$, but the saturation gradient will begin to change.

Tavassoli et al. (2005) pointed out that the oil mobility and hence diffusion coefficient Λ_n approaches zero at $X=0$, which must be compensated by an infinite saturation gradient. Their product is however finite and constant during early time (McWhorter and Sunada 1990). This is however only the case for strongly water-wet media, but not mixed-wet media where oil still has mobility at the saturation where SI stops.

2.3 Numerical implementation

Discretization procedures of the early and full time solutions are outlined. They were implemented in Matlab. The Z -axis was discretized into $N=1500$ cells of fixed width ΔZ having center positions $Z_i = (i-1/2)\Delta Z$. In the early-time system the maximum Z value was set sufficient to satisfy the initial condition (see Section 3.2). In the full-time system the initial time was set in agreement with this limit, with the maximum Z subsequently obeying $Z_{\max} = 1/Y$.

2.3.1 Early time system discretization

Let saturation S_n in cell i be denoted S_i , and let $i=0$ be a ghost cell outside the inlet with saturation $S_0 = 1$. The initial condition is implemented by setting $S_{N+1} = 0$. A finite difference approximation of Eq. (11) results in:

$$\begin{aligned} -\frac{2}{\Delta Z} \left[\Lambda_{i+0.5} \frac{(S_{i+1} - S_i)}{\Delta Z} - \Lambda_{i-0.5} \frac{(S_i - S_{i-1})}{\Delta Z} \right] \\ = \frac{Z_i(S_i - S_{i-1})}{\Delta Z}, \quad (i = 1 : N) \end{aligned} \quad (21)$$

where $\Lambda_{i+0.5} = \Lambda_n(0.5(S_i + S_{i+1}))$. Eq. (21) can also be written as:

$$\begin{aligned} F_i(S_{i-1}, S_i, S_{i+1}) \\ := [\Lambda_{i+0.5}(S_{i+1} - S_i) - \Lambda_{i-0.5}(S_i - S_{i-1})] \\ + \frac{Z_i \Delta Z}{2} (S_i - S_{i-1}) = 0, \quad (i = 1 : N) \end{aligned} \quad (22)$$

At $i=1$, apply $S_{i-1} = 1$, while at $i=N$ apply $S_{i+1} = 0$. The N equations defined by $F_i = 0$ are solved using linearization with Newton-Raphson's method:

$$\begin{aligned} F_i^{k+1} = F_i^k + \sum_j \left(\frac{\partial F_i}{\partial S_j} \right)^k \Delta S_j^k = 0 \\ \Delta S_j^k = S_j^{k+1} - S_j^k, \quad (i = 1 : N) \end{aligned} \quad (23)$$

This linear system is tridiagonal wrt ΔS_j^k and can be solved by direct or indirect methods. When the iterations do not affect the coefficients or solution estimate further, the solution has converged.

2.3.2 Full time system discretization

Saturation S_n in cell i at old time step n is denoted S_i^n . Evaluation at new time step $n+1$ is not explicitly indicated for $S_i, S_{i+1}, Y, \Lambda_{i\pm 0.5}, \Delta Z$. The time steps $\Delta Y = Y^{n+1} - Y^n$ are assumed fixed. Eq. (18) can then be discretized fully implicit as:

$$\frac{S_i - S_i^n}{\Delta Y} = \frac{2[\Lambda_{i+0.5}(S_{i+1} - S_i) - \Lambda_{i-0.5}(S_i - S_{i-1})]}{Y(\Delta Z)^2} \quad (24)$$

define $\gamma_{YZ} = 2\Delta Y/Y(\Delta Z)^2$ and write Eq. (24) as a function F_i to be zero. The boundary conditions are included the same way as for the early time solution, while the initial condition is included as $S_i^0 = 0$.

$$\begin{aligned} F_i(S_{i-1}, S_i, S_{i+1}) \\ := (S_i - S_i^n) + \gamma_{YZ} \Lambda_{i-0.5} (S_i - S_{i-1}) \\ - \gamma_{YZ} \Lambda_{i+0.5} (S_{i+1} - S_i) = 0, \quad (i = 1 : N) \end{aligned} \quad (25)$$

This system is solved with Newton-Raphson's method each time step.

3. Results and discussion

3.1 Saturation function correlations

The applied saturation function correlations are given by:

$$k_{ri} = k_{ri}^* (S_i)^{n_i}, \quad n_i = n_{i1} S + n_{i2} (1 - S), \quad (i = o, w) \quad (26)$$

$$J = -J_1 \ln \frac{S}{S_{eq}} + J_2 \ln \frac{1-S}{1-S_{eq}} \quad (27)$$

where S denotes scaled mobile saturations and S_{eq} the highest imbibing mobile saturation (where scaled imbibing saturation is $S_n = 1$). Note that $S_n = S/S_{eq}$. k_{ri}^* are relative permeability end points, n_i saturation dependent Corey exponents (varying between n_{i1} and n_{i2}) and J_1, J_2 are J -function fitting parameters. The definition of the function Λ results in:

$$\Lambda = \frac{J_2 k_{ro}^* S^{n_w-1} (1-S)^{n_o} \frac{J_1}{J_2} + S^{n_w} (1-S)^{n_o-1}}{\sqrt{\frac{\mu_o}{\mu_w}} \frac{S^{n_w} + \frac{k_{ro}^* \mu_w}{k_{rw}^* \mu_o} (1-S)^{n_o}}{S^{n_w} + \frac{k_{ro}^* \mu_w}{k_{rw}^* \mu_o} (1-S)^{n_o}}} \quad (28)$$

Λ_n is simply Λ divided by its mean $\bar{\Lambda}$ over the imbibing saturation interval. The shape of Λ_n is determined by the relative permeabilities, J -function and the mobility ratio $M = (k_{ro}^* \mu_w)/(k_{rw}^* \mu_o)$. Other parameters (such as $J_2 k_{ro}^*/\sqrt{\mu_o/\mu_w}$ which cancels during normalization) do not affect Λ_n which has magnitude 1 but affect how the scaled solutions are converted back to unscaled dimensions.

To quickly assess the diffusion coefficients Λ_n a quantification is made of the fraction of the coefficient shifted to the

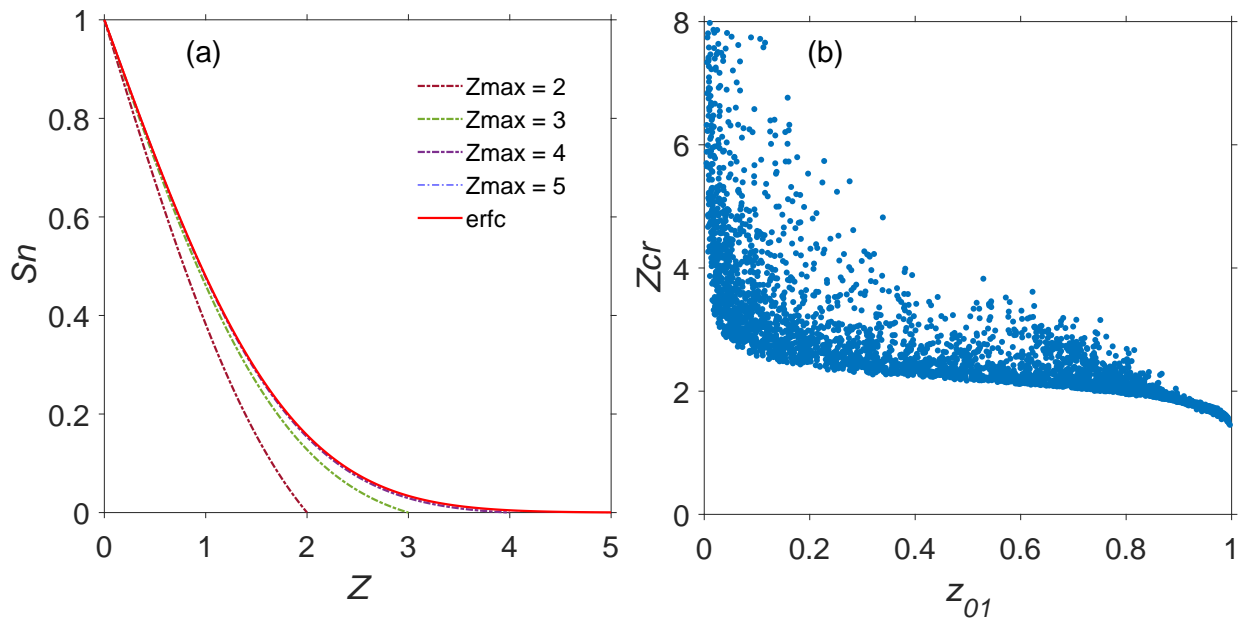


Fig. 1. Numerical solutions of Eq. (11) (a) to obtain the early time solution $S_n(Z)$ for $\Lambda_n = 1$ on intervals $0 < Z < Z_{\max}$ for different choices of Z_{\max} . Selecting Z_{\max} too low gives incorrect solutions, while sufficiently high values reproduce the correct analytical solution (erfc). Critical values Z_{cr} (b) are plotted for different Λ_n (5,500 functions from Andersen (2022)) against their fraction z_{01} .

right-hand side, defined by z_{01} :

$$z_{01} = \frac{\int_{S_n=0.5}^1 \Lambda_n dS_n}{\int_{S_n=0}^1 \Lambda_n dS_n}, \quad (0 < z_{01} < 1) \quad (29)$$

Such a fraction (or more detailed description of the shape of Λ_n) determines most of the resulting recovery behavior (Andersen, 2021, 2022).

3.2 Reasonable initial range of Z

The simplest solution to the system Eqs. (11) and (12) is setting $\Lambda_n = 1$ constant. This results in the well known erfc solution (Boltzmann, 1878; Cussler, 2009), which adapted to our system is:

$$S_n = \operatorname{erfc}\left(\frac{Z}{2}\right), \quad (0 < Z < \infty) \quad (30)$$

This profile does not actually go to zero at a finite distance, but quickly approaches extremely small values. A front at $Z_{\max} = 5$ was defined such that 0.9999 of the imbibed profile is behind this position (for comparison 0.9995 is behind $Z = 4.5$).

The system Eqs. (11) and (12) was solved with $\Lambda_n = 1$ to demonstrate the importance of selecting a sufficiently large Z_{\max} , see Fig. 1(a). If Z_{\max} is sufficiently large (4 or higher) identical solutions $S_n(Z)$ are obtained obeying the same initial condition and obtaining this value $S_n = 0$ at large enough Z . The analytical erfc solution is reproduced. However, if Z_{\max} is selected too small (2 or 3 in this example), the solution is forced to equal the initial condition at a finite rather than infinite distance. This does not produce the correct early time solution.

When comparing general solutions to the erfc solution

there are two trends. Coefficients Λ_n shifted right (high z_{01}) imbibe more after the same time T (or Y) due to increasing A with z_{01} but have more compact saturation profiles (higher RF_{cr}) (Andersen, 2022). Oppositely, coefficients shifted left (low z_{01}) imbibe less (lower A) but have low average saturation of the imbibing profile (low RF_{cr}). In both cases, the two cancelling effects suggest that the fastest saturation may not have travelled very differently compared to the erfc solution. Based on a dataset of 5,500 realistic Λ_n coefficient functions Z_{cr} was calculated analytically and plotted against the corresponding z_{01} in Fig. 1(b). For most cases, Z_{cr} is between 1.5 and 5, with Z_{cr} decreasing as z_{01} increases. However, at low $z_{01} < 0.2$ it may be necessary to use a high $Z_{cr} \approx 10$.

3.3 Investigation of imbibition behavior

3.3.1 Input parameters

Input relative permeabilities and J -function were based on experimentally measured imbibition curves from Kleppe and Morse (1974). See Fig. 2 and the related parameters in Table 1. Their data were strongly water-wet (SWW). To consider behavior also for mixed-wet (MW) cases a modified J -function was added where S_{eq} (scaled saturation S where J is zero) is changed from 0.999 (SWW) to 0.75 (MW), with other parameters fixed.

3.3.2 Diffusion coefficients and early time solution

Six oil-to-water mobility ratios M were considered (higher and lower than the reference value of 4.7) for both wettability cases to vary the shape of the diffusion coefficient Λ_n , see Fig. 3. Higher mobility ratio M causes the diffusion coefficients to be shifted to higher saturations as quantified by higher values

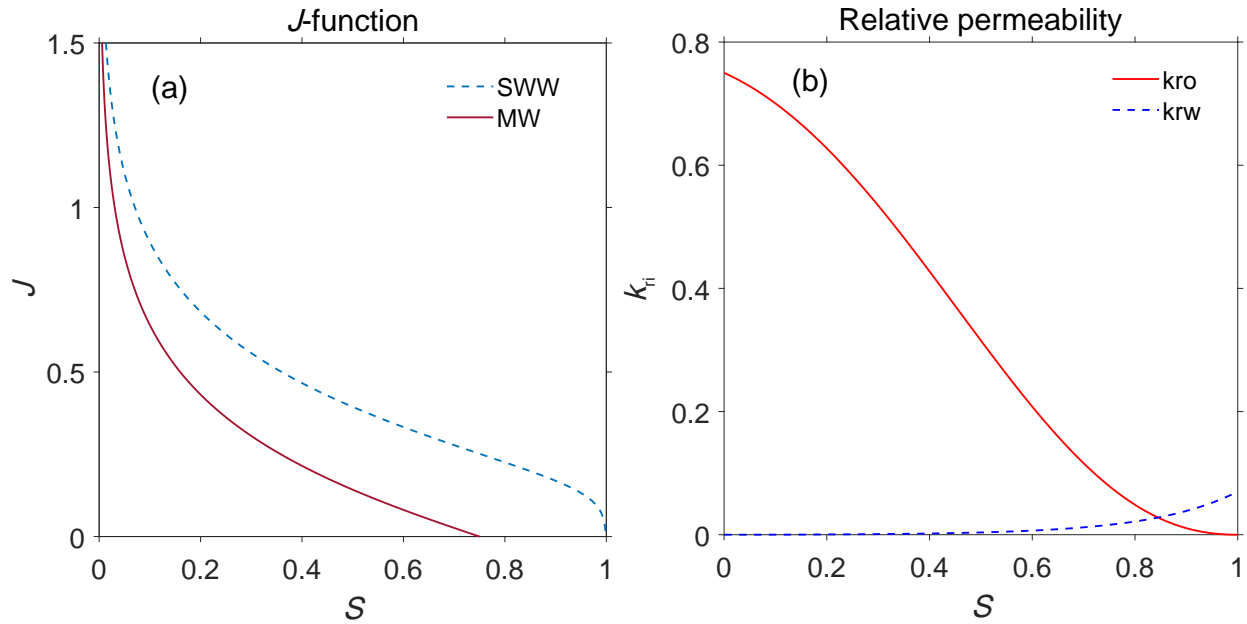


Fig. 2. Saturation functions adapted to measured functions from Kleppe and Morse (1974) on strongly water-wet media (J -function (a) and relative permeabilities (b)). The MW J -function is based on shifting the crossing point of the SWW curve to $S_{eq} = 0.75$. The functions are shown on the full mobile saturation interval $0 < S < 1$.

Table 1. Saturation function- and other parameters used to define Λ_n , based on Kleppe and Morse (1974).

Parameters	n_{w1}	n_{w2}	n_{o1}	n_{o2}	k_{rw}^*	k_{ro}^*	$\mu_o(cP)$	$\mu_w(cP)$	M	J_1	J_2	S_{eq}
Value	6	2.5	2	0.5	0.07	0.75	2.3	1	4.7	0.3	0.03	0.999

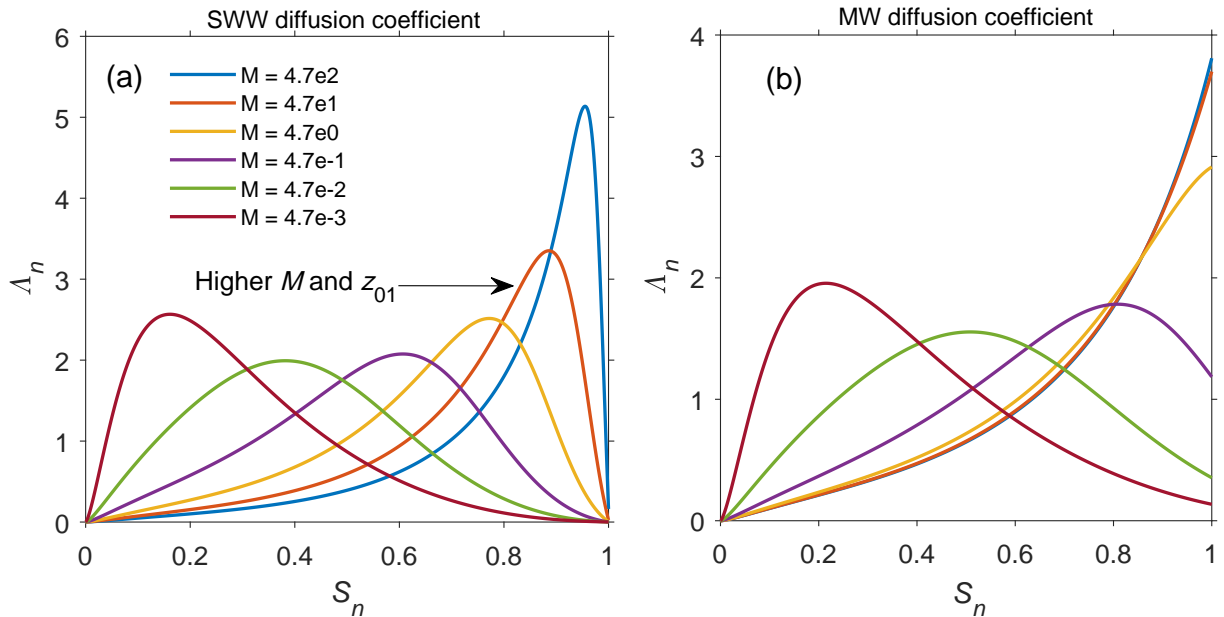
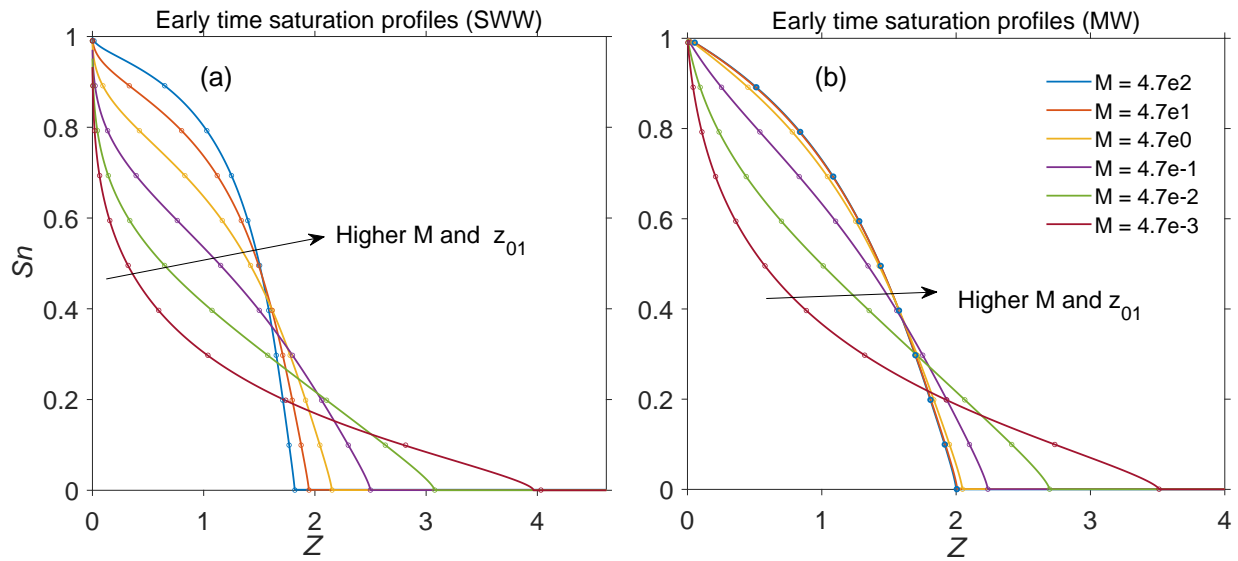


Fig. 3. Scaled diffusion coefficients Λ_n for SWW (a) and MW (b) cases for six different mobility ratios M varying five orders of magnitude. The functions are shown on the imbibing saturation interval $0 < S_n < 1$.

Table 2. Quantified diffusion coefficients and imbibition behavior for different mobility ratios and wettabilities.

M	SWW ($S_{eq} = 0.999$)					MW ($S_{eq} = 0.75$)				
	z_{01}	A	RF_{cr}	Z_{cr}	$RF_{cr}Z_{cr}$	z_{01}	A	RF_{cr}	Z_{cr}	$RF_{cr}Z_{cr}$
$4.7e2$	0.925	0.669	0.735	1.82	1.34	0.859	0.655	0.653	2.01	1.31
$4.7e1$	0.885	0.647	0.664	1.95	1.29	0.857	0.654	0.651	2.01	1.31
$4.7e0$	0.800	0.612	0.568	2.16	1.23	0.843	0.649	0.634	2.05	1.30
$4.7e-1$	0.603	0.563	0.451	2.50	1.13	0.760	0.622	0.556	2.24	1.25
$4.7e-2$	0.307	0.500	0.325	3.08	1.00	0.526	0.563	0.418	2.70	1.13
$4.7e-3$	0.133	0.432	0.214	4.03	0.86	0.267	0.490	0.279	3.51	0.98

**Fig. 4.** Early time saturation profiles $S_n(Z)$ for SWW (a) and MW (b) cases for six different mobility ratios. The full lines represent numerical solutions of the early time differential equation, while the circles represent the semi-analytical solution (only a few points shown) included for validation.

of z_{01} (Table 2). CO_2 and H_2 have high mobility compared to water (high M) and their spontaneous displacement by water imbibition can be considered represented under the high M cases. Water is considered strongly or preferentially wetting compared to H_2 and CO_2 in sandstone aquifers but can be less wetting in reservoirs where polar oils have aged the rock surface (Iglauer et al. 2021).

The early time saturation profile for each diffusion coefficient is plotted as $S_n(Z)$ for MW and SWW cases in Fig. 4, using all six mobility ratios. Numerical solutions of Eq. (11) (full lines) are validated by the semi-analytical solution Eq. (14) (circles). Z_{\max} was set to 5 which was sufficient to achieve the initial condition $S_n = 0$ ahead of the imbibition front for all cases. Z_{cr} can be determined from where the saturation profile reaches the initial condition and then the critical time is found as $T_{cr} = 1/Z_{cr}^2$, see Eq. (14). Equivalently, $Y_{cr} = 1/Z_{cr}$.

For both wetting states (or a given set of saturation functions), the impacts of increasing the oil-to-water mobility ratio are (a) the front Z_{cr} reaching a shorter distance, (b)

higher average saturation (equal to RF_{cr}) within the imbibition profile, (c) higher total amount imbibed, as quantified by larger imbibition rate coefficient A , or the product $RF_{cr}Z_{cr}$ (the area of the imbibed profile). This is also quantified in Table 2. Note that the profile area $RF_{cr}Z_{cr}$ increases although the distance Z_{cr} decreases. The strong trend in $RF_{cr}Z_{cr}$ with z_{01} is expected since the imbibition coefficient A has been shown to correlate predominantly with z_{01} regardless of the saturation functions and viscosities applied to generate the Λ_n (Andersen, 2022). The lower Z_{cr} with higher z_{01} is consistent with the general trend in Fig. 1(b): The z_{01} between 0.1 and 0.9 and Z_{cr} from 2 to 4 corresponds well with the rest of the data.

Considering SWW states, Λ_n is zero at $S_n = 1$ by definition (the capillary pressure goes to zero at the residual oil saturation). To have a finite imbibition rate q_0 , see Eq. (20), the inlet saturation gradient must be infinite, which is seen in Fig. 4 for all mobility ratios. However, at more favorable (high) M the saturation gradient declines in magnitude very quickly when distancing from the inlet. For the MW states, Λ_n is nonzero at $S_n = 1$ and the finite imbibition rate requires a

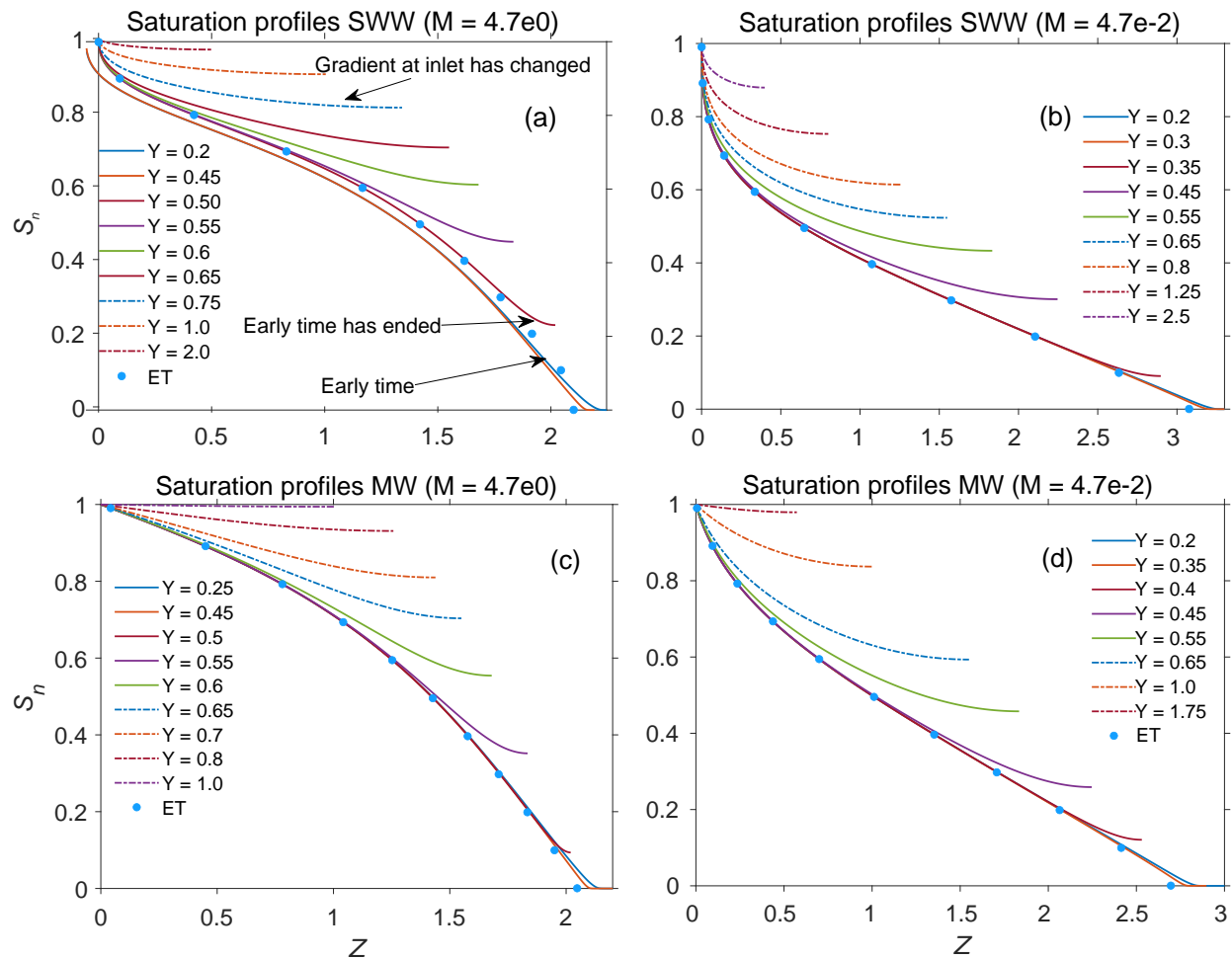


Fig. 5. Saturation profiles $S_n(Z)$ at different times $Y = T^{0.5}$ shown for SWW ((a) and (b)) and MW ((c) and (d)) cases with high ((a) and (c)) and low ((b) and (d)) mobility ratio M . The early time solution calculated semi-analytically is included for comparison.

finite inlet saturation gradient, which is clearly seen for all cases. A finite saturation gradient at the inlet is also seen for the erfc solution in Fig. 1, which is based on a constant (and thus finite) coefficient $\Lambda_n = 1$ at the inlet. However, the tendency for a gradient to be sharp in the surroundings of the inlet seems to be how much mobility there is overall at high saturations. If the coefficient is shifted to high saturations (high z_{01}), generally a flatter saturation profile (low saturation gradient) is observed.

If the mobility ratio is sufficiently high, the mobility of oil can be ignored compared to that of water and $\Lambda_n \propto k_{rw} J'$. The SWW coefficients in Fig. 3 are relatively distinct although the two cases with highest M are more comparable. At high water saturations the oil mobility goes to zero and it cannot be ignored compared to the water mobility. For the MW cases, however, the three diffusion coefficients with highest mobility ratio are almost identical and provide almost overlapping saturation profiles. Compared to the SWW case only one parameter was changed which is where the J -function is zero. However, this causes the imbibition saturation range to cover saturations where oil has finite and much higher mobility. Under these conditions the oil mobility can be neglected at

lower (but sufficiently high) mobility ratios.

3.3.3 Full time solution

Next, consider the full-time system Eqs. (18) and (19) and its solutions. Time steps ΔY smaller than $Y_{cr} = 1/Z_{cr}$ should be used to ensure the early time solution is captured. From Fig. 1 and Fig. 4 it is found that $\Delta Y < 1$ ensures this. Practically, to get accurate derivatives more time steps were necessary. Simulation was performed until $Y = 2.5$ using 500 time steps, i.e., $\Delta Y = 0.005$. Two SWW and two MW cases were considered with mobility ratios M equal 4.7e-2 and 4.7e0. The saturation profiles $S_n(Z)$ are shown at different times Y in Fig. 5.

At the two lowest times Y the profiles (blue and red lines) overlap and are identical to the unique early time solution (also shown as blue circles calculated by the semi-analytical solution for validation).

The closed boundary at $Z = 1/Y$ moves closer to the early time profile and the vertical axis with time. When the closed boundary meets the saturation profile, the saturation profile covers a shorter interval on the Z -axis, but the saturations on that interval increase as the imbibing profile cannot pass.

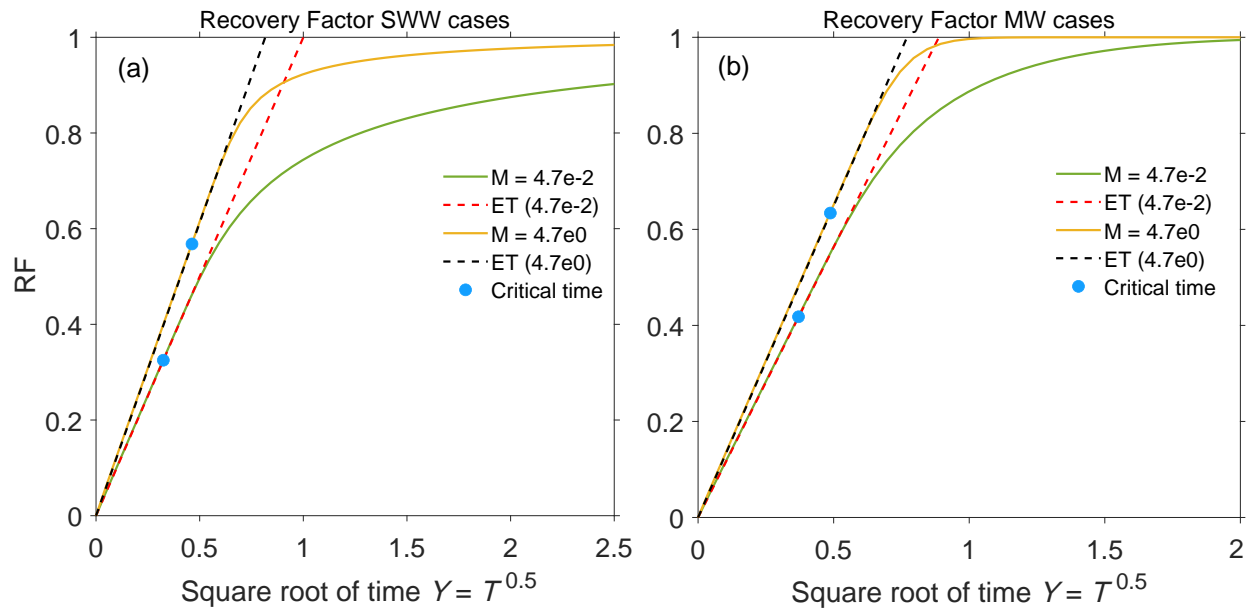


Fig. 6. Recovery factor plotted against Y for SWW (a) and MW (b) cases for two mobility ratios M equal $4.7e-2$ and $4.7e0$. The dashed lines indicate the extended early time solution $RF = RF_{cr} Z_{cr} Y$. The critical time points ($Y = 1/Z_{cr}$, $RF = RF_{cr}$) are shown for each curve.

The brown full-line curve is the first to deviate from the early time profile and marks that the critical time $Y_{cr} = T_{cr}^{0.5}$ has passed. An interesting observation is that although the profile has interacted with the closed boundary, the impact is local and most of the profile that is not near the closed boundary looks like the early time solution. The late time (post critical) profiles terminate at saturations higher than the initial condition, with a zero saturation gradient indicating the closed boundary. Notably, the interaction with the closed boundary travels as a wave towards the inlet, showing deviation from the early time profile on a greater interval with time.

Eventually the deviation is noticeable across the full profile, including the gradient at the inlet position $Z = 0$ (the inlet saturation itself is fixed). The profiles where this is visible are dashed. The change in inlet saturation gradient $\partial_z S_n|_{Z=0}$ marks a change in imbibition rate from being proportional to $T^{-0.5} = 1/Y$ (and thus recovery being proportional to Y) to declining faster as the magnitude of $\partial_z S_n|_{Z=0}$ decreases, see Eq. (20).

To evaluate the relation between the saturation profiles and recovery behavior, recovery factor is plotted against Y in Fig. 6. Of main interest is to determine what controls when recovery stops being linear with square root of time, i.e. linear with Y .

First of all, note that the saturation profiles in Fig. 5 have encountered the closed boundary at $Y = 0.5, 0.35$ (SWW, high and low M), 0.5 and 0.4 (MW, high and low M), roughly defining the critical times (exact times are indicated in Fig. 6). However, the corresponding times where a clear visual separation can be detected between the recovery curve and the straight line (extended from early time) is at $Y = 0.65, 0.5$ (SWW, high and low M), 0.65 and 0.55 (MW, high and low M). In all the four cases, the onset occurs at a

delay of $Y_{onset} - Y_{cr} \approx 0.15$ and the difference in recovery is $RF_{onset} - RF_{cr} \approx 0.15$ to 0.20 . Such consistent delays in deviation from square root of time recovery compared to the critical time were reported for large datasets of simulations in Andersen (2021, 2022). Andersen (2022) also showed that experimental early time 1D COUSI data from Fischer et al. (2008) were linear when plotted against square root of time. Li et al. (2006) tested 1D water-oil imbibition and their data showed that the front met the closed boundary at $90 \text{ sec}^{0.5}$, while recovery was linear with square root of time until $110 \text{ sec}^{0.5}$. They could match both features with simulation.

The onset times correspond very well with the times of the last profiles which have similar inlet saturation gradient as the early time solution (the full line with highest saturations): $Y = 0.65, 0.55$ (SWW, high and low M), 0.6 and 0.55 (MW, high and low M). This confirms that it is not the interaction with the closed boundary, but the subsequent interaction with the inlet boundary that determines when the square root of time recovery behavior ends.

3.4 Interpretation of experimental data

Ruth et al. (2016) measured in-situ saturation profiles and production vs time during 1D COUSI. Before interpretation, data consistency was checked such that the recovery based on both saturation profiles and production became zero at zero time and that the recovery from both sources overlapped at identical times. A corrected time was required by shifting the square root of time as $t_{cor}^{0.5} = t^{0.5} + \Delta t^{0.5}$. $\Delta t^{0.5}$ was equal $0.7 \text{ min}^{0.5}$ for saturation profile data and $-1.1 \text{ min}^{0.5}$ for production data. Ultimate oil production was set slightly higher than the last observed cumulative production when defining recovery.

Four saturation profiles were from early time and a fifth at late time. Data from six core locations were reported. The ea-

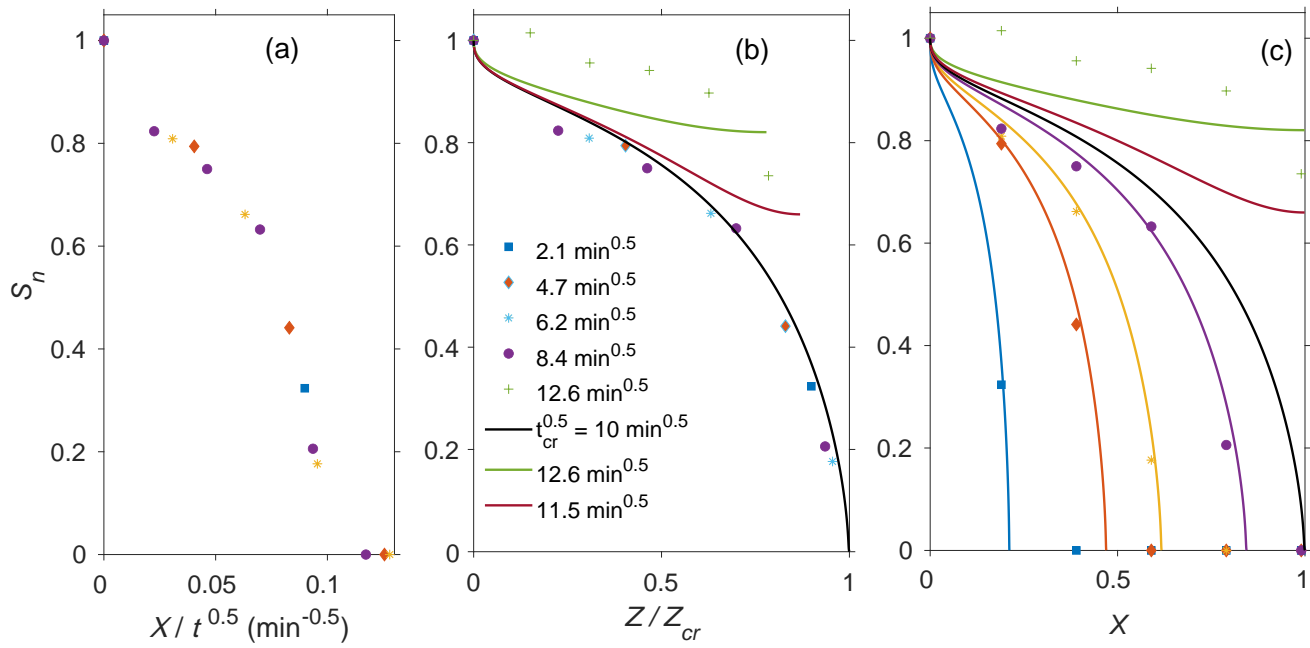


Fig. 7. In situ saturation data (points) from Ruth et al. (2016) plotted against $X/t^{0.5}$ (a), Z/Z_{cr} (b) and X (c). Full lines indicate simulations.

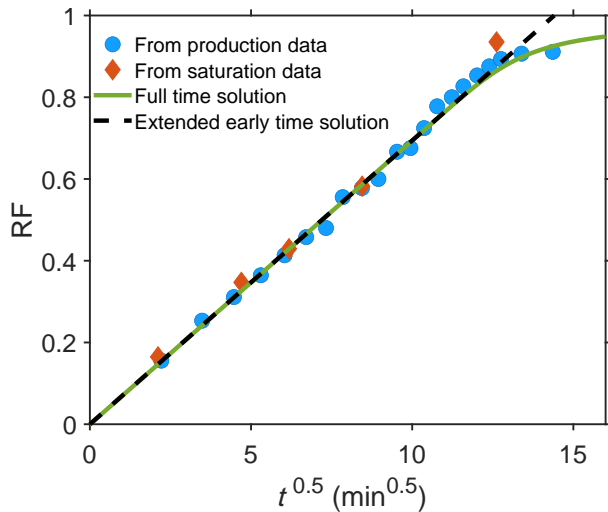


Fig. 8. Recovery data from Ruth et al. (2016) based on oil production and in situ saturation profiles compared with early and full time solutions.

Early time data were first plotted against $X/t^{0.5}$ (t in min) which collected the curves to one spatial profile $S_n(X/t^{0.5})$, see Fig. 7(a). The critical value where the curves approach zero saturation was found as $(X/t^{0.5})_{cr} = 1/t_{cr}^{0.5} \approx 0.10$ and used to define the critical (root of) time: $t_{cr} = (1/0.10)^2 = (10 \text{ min}^{0.5})^2 = 100 \text{ min}$.

The spatial axis was then scaled wrt the critical value, yielding Z/Z_{cr} . This plot was matched with numerical simulation in Fig. 7(b) by selecting a SWW function Λ_n (to capture the strong gradient at the inlet), shifted to high saturations (to capture the high average saturation in the profile), but with somewhat limited mobility at the highest saturations (to

capture that the highest saturations travel slowly). The curve fits the four early time profiles well.

Two late time profiles were also generated: one predicting the experimental data at $12.6 \text{ min}^{0.5}$ and one at $11.5 \text{ min}^{0.5}$ (after the critical time). Both these curves differ from the early time curve, but the $12.6 \text{ min}^{0.5}$ curve is the first to show deviation near the inlet, suggesting recovery should stay proportional to square root of time until $12.6 \text{ min}^{0.5}$, a significant period later than the critical time $10 \text{ min}^{0.5}$, almost an hour delay.

That predicted delay is confirmed by the recovery data in Fig. 8. The recovery at the critical time is ~ 0.7 , but simulated deviation from the straight line only occurs at recovery of 0.83 . The experimental data suggests the linear behavior to last even longer (~ 0.9 recovery).

Spatial profiles in regular spatial coordinates X are also shown in Fig. 7(c). The model solution simply expands the same invariant profile until meeting the no-flow boundary and then obtains a zero saturation gradient at $X = 1$ with increasing saturations. The early time solution meeting the boundary at $t = 10 \text{ min}^{0.5}$ is confirmed in this plot.

3.5 Comparison with traditional approaches

The standard way of considering the diffusion system is with variables position x and time t . That approach may however provide little insight. By first scaling the system to variables X and T the solution only depends on whether the coefficient Λ_n is shifted to low or high saturations (Andersen 2022). By further presenting the system in the early time form the solution is invariant in shape and can thus determine the profile at any early time, as a simple expansion, as well as directly calculating the critical time when this solution form ceases to be valid (from the output Z_{cr}), as illustrated in the

previous section.

The full-time solution expressed with Z , Y preserves the invariant solution form until late time and is independent of Y initially but captures the transition when the imbibition profile meets the closed boundary. At early time less volume imbibes per unit time T , however, the same amount imbibes per unit Y , which is more visual and intuitive. For example, recovery is linear against Y while it is difficult to present recovery data visually in a linear time plot. Equivalently, early time imbibition profiles at same increments in Y have same difference in imbibed volume.

A practical challenge of the Z -variable is that the solution on the applied range $0 < Z < Z_{\max}$ the applied range must contain the initial condition. For diffusion coefficients shifted to high saturations (high z_{01}) lower Z_{\max} could be used, even lower than the erfc solution. However, for coefficients shifted to low saturations (low z_{01}) high Z_{\max} are necessary. From our analysis, accurate estimates of $Z_{\max} > Z_{cr}$ can be made for any diffusion coefficient resulting in correct early time solutions.

4. Conclusions

The 1D counter-current spontaneous imbibition problem was considered, first in a general scaled form and then translated to a new set of variables. At early time only the variable $Z = X/T^{0.5}$ is needed to determine the unique solution $S_n(Z)$, while at late times it depends on a second variable which was selected to be $Y = T^{0.5}$. Early and full-time systems were investigated. Diffusion coefficients Λ_n were characterized by the fraction z_{01} of their area on the top-side saturation interval. High oil-to-water mobility ratios correspond to high z_{01} . The following was concluded:

- 1) When increasing M or z_{01} the impacts on the early time profile are: the front position Z_{cr} travels shorter; the imbibition profile obtains higher average saturation; higher total amount imbibes.
- 2) The imbibition rate at any time is determined by Λ_n times $\partial_Z S_n$, both evaluated at the inlet, times inverse square root of time. For SWW cases the coefficient is zero since capillary pressure is zero at immobile oil saturation, yielding an infinite saturation gradient. For MW cases the coefficient is nonzero since capillary pressure is zero at a saturation where both fluids are mobile. This results in a finite saturation gradient.
- 3) At early time $S_n(Z)$ is invariant, hence the inlet $\partial_Z S_n$ is constant and imbibition rate remains proportional to inverse square root of time. At critical time, water meets the no-flow boundary. $S_n(Z)$ begins deviating from the early time profile, first at the no-flow boundary, then towards the inlet. After sufficient time the inlet $\partial_Z S_n$ is affected, causing imbibition rate to decline faster than by inverse square root of time. Since the interaction with the inlet boundary, not the closed boundary, determines imbibition rate; recovery can stay linear with square root of time much longer than the early-time period.
- 4) At high M the mobility of oil becomes negligible compared to that of water and Λ_n becomes independent of M . So do the resulting solutions. For SWW cases the

mobility of oil goes to zero at high saturations making it very difficult to be fully negligible. However, for MW cases oil mobility stays finite and the solutions become insensitive to M at much lower M .

Acknowledgements

The author acknowledges the Research Council of Norway and the industry partners of NCS2030 – RCN project 331644 – for their support. Jassem Abbasi is acknowledged for good discussions about the behavior and discretization of the differential equations.

Conflict of interest

The author declares no competing interest.

Open Access This article is distributed under the terms and conditions of the Creative Commons Attribution (CC BY-NC-ND) license, which permits unrestricted use, distribution, and reproduction in any medium, provided the original work is properly cited.

References

- Andersen, P. Ø. A semi-analytical solution for shale gas production from compressible matrix including scaling of gas recovery. *Journal of Natural Gas Science and Engineering*, 2021, 95: 104227.
- Andersen, P. Ø. Early-and late-time prediction of counter-current spontaneous imbibition, scaling analysis and estimation of the capillary diffusion coefficient. arXiv preprint arXiv, 2022: 2211.07571.
- Andersen, P. Ø., Nesvik, E. K., Standnes, D. C. Analytical solutions for forced and spontaneous imbibition accounting for viscous coupling. *Journal of Petroleum Science and Engineering*, 2020, 186: 106717.
- Andersen, P. Ø., Salomonsen, L., Sleveland, D. S. Characteristic forced and spontaneous imbibition behavior in strongly water-wet sandstones based on experiments and simulation. *Energies*, 2022, 15(10): 3531.
- Bennion, D. B., Bachu, S. Drainage and imbibition CO₂/brine relative permeability curves at reservoir conditions for carbonate formations. Paper SPE 134028 Presented at SPE Annual Technical Conference and Exhibition, Florence, Italy, 19-22 September, 2010.
- Boltzmann, L. Zur integration der diffusionsgleichung bei variabeln diffusionscoefficienten. *Annalen der Physik*, 1894, 289(13): 959-964.
- Bourbiaux, B. J., Kalaydjian, F. J. Experimental study of cocurrent and countercurrent flows in natural porous media. *SPE Reservoir Engineering*, 1990, 5(3): 361-368.
- Cai, J., Yu, B. A discussion of the effect of tortuosity on the capillary imbibition in porous media. *Transport in Porous Media*, 2011, 89(2): 251-263.
- Carslaw, H. S., Jaeger, J. C. *Conduction of heat in solids*. Oxford, UK. Clarendon Press 1947.
- Crank, J. *The Mathematics of Diffusion*. Oxford University Press, 1979.
- Crank, J., Henry, M. E. Diffusion in media with variable properties. Part I. The effect of a variable diffusion coefficient on the rates of absorption and desorption. *Transactions*

- of the Faraday Society, 1949, 45: 636-650.
- Cussler, E. L. *Diffusion: Mass Transfer in Fluid Systems*. Cambridge University Press, 2009.
- Fischer, H., Wo, S., Morrow, N. R. Modeling the effect of viscosity ratio on spontaneous imbibition. *SPE Reservoir Evaluation & Engineering*, 2008, 11(3): 577-589.
- Iglauer, S., Ali, M., Keshavarz, A. Hydrogen wettability of sandstone reservoirs. implications for hydrogen geostorage. *Geophysical Research Letters*, 2021, 48(3): e2020GL090814.
- Khan, A. S., Siddiqui, A. R., Abd, A. S., et al. Guidelines for numerically modeling co-and counter-current spontaneous imbibition. *Transport in Porous Media*, 2018, 124(3): 743-766.
- Kleppe, J., Morse, R. A. Oil production from fractured reservoirs by water displacement. Paper SPE 5084 Presented at Fall meeting of the Society of Petroleum Engineers of AIME, Houston, Texas, US, 6-9 October, 1974.
- Larsson, H. On the use of Boltzmann's transformation to solve diffusion problems. *Calphad*, 2021, 73: 102261.
- Le Guen, S. S., Kovscek, A. R. Nonequilibrium effects during spontaneous imbibition. *Transport in Porous Media*, 2006, 63(1): 127-146.
- Li, Y., Ruth, D., Mason, G., et al. Pressures acting in counter-current spontaneous imbibition. *Journal of Petroleum Science and Engineering*, 2006, 52(1-4): 87-99.
- Ma, S., Morrow, N. R., Zhang, X. Generalized scaling of spontaneous imbibition data for strongly water-wet systems. *Journal of Petroleum Science and Engineering*, 1997, 18(3-4): 165-178.
- Makhanov, K., Habibi, A., Dehghanpour, H., et al. Liquid uptake of gas shales: A workflow to estimate water loss during shut-in periods after fracturing operations. *Journal of Unconventional Oil and Gas Resources*, 2014, 7: 22-32.
- March, R., Doster, F., Geiger, S. Accurate early-time and late-time modeling of countercurrent spontaneous imbibition. *Water Resources Research*, 2016, 52(8): 6263-6276.
- Mattax, C. C., Kyte, J. R. Imbibition oil recovery from fractured, water-drive reservoir. *SPE Journal*, 1962, 2(2): 177-184.
- McWhorter, D. B., Sunada, D. K. Exact integral solutions for two-phase flow. *Water Resources Research*, 1990, 26(3): 399-413.
- Meng, Q., Cai, Z., Cai, J., et al. Oil recovery by spontaneous imbibition from partially water-covered matrix blocks with different boundary conditions. *Journal of Petroleum Science and Engineering*, 2019, 172: 454-464.
- Morrow, N. R., Mason, G. Recovery of oil by spontaneous imbibition. *Current Opinion in Colloid & Interface Science*, 2001, 6(4): 321-337.
- Qiao, Y., Andersen, P. Ø., Evje, S., et al. A mixture theory approach to model co-and counter-current two-phase flow in porous media accounting for viscous coupling. *Advances in Water Resources*, 2018, 112: 170-188.
- Ruth, D. W., Fernø, M. A., Haugen, Å., et al. Matching experimental saturation profiles by numerical simulation of combined and counter-current spontaneous imbibition. Paper SCA2016-005 Presented at the International Symposium of the Society of Core Analysts, Snowmass, Colorado, USA, 20-23 August, 2016.
- Schmid, K. S., Geiger, S. Universal scaling of spontaneous imbibition for arbitrary petrophysical properties: Water-wet and mixed-wet states and Handy's conjecture. *Journal of Petroleum Science and Engineering*, 2013, 101: 44-61.
- Stenlund, H. Three methods for solution of concentration dependent diffusion coefficient. *Visilab Signal Technologies Oy*, Finland, 2011.
- Sæle, A., Graue, A., Alcorn, Z. P. Unsteady-state CO₂ foam injection for increasing enhanced oil recovery and carbon storage potential. *Advances in Geo-Energy Research*, 2022, 6(6): 472-481.
- Tantciura, S., Qiao, Y., Andersen, P. Ø. Simulation of counter-current spontaneous imbibition based on momentum equations with viscous coupling, Brinkman terms and compressible fluids. *Transport in Porous Media*, 2022, 141(1): 49-85.
- Tavassoli, Z., Zimmerman, R. W., Blunt, M. J. Analytic analysis for oil recovery during counter-current imbibition in strongly water-wet systems. *Transport in Porous Media*, 2005, 58(1): 173-189.
- Wang, X., Sheng, J. J. A self-similar analytical solution of spontaneous and forced imbibition in porous media. *Advances in Geo-Energy Research*, 2018, 2(3): 260-268.
- Zhou, Y., You, L., Kang, Y., et al. Influencing factors and application of spontaneous imbibition of fracturing fluids in lacustrine and marine shale gas reservoir. *Energy & Fuels*, 2022, 36(7): 3606-3618.